Least Squares DAS to geophone transform

Jorge E. Monsegny, Kevin Hall, Daniel Trad and Don C. Lawton

ABSTRACT

Distributed acoustic sensing uses optical fibre to measure strain or strain rate along to the fibre direction. In contrast, geophones are equipped with a spring-mass system that measures the particle velocity in the direction of this spring-mass system. The strain rate estimated by distributed acoustic sensing is related to the total displacement of a section of the fibre called gauge length. By using this link between strain rate and displacement we propose a least squares inversion scheme to obtain the particle velocity along the fibre from strain rate in a distributed acoustic sensing system. We test this least squares transformation with data from the Containment and Monitoring Institute Field Research Station in Alberta, Canada. We found that the transformed traces are very similar to a filtered version of the corresponding geophone ones, in particular at early times.

INTRODUCTION

Distributed acoustic sensing is a seismic monitoring technology that uses optical fibre to obtain the strain, or strain rate, related to the fibre deformation by a passing seismic wave (Daley et al., 2013). Basically, a laser pulse probes different sections of the fibre. Some of the laser energy is backscattered and detected by the DAS measuring device, usually called interrogator. In the absence of any disturbance that can deform the fibre, the backscattering is static. When a seismic event deforms a section of the fibre, the backscattering changes for this section and the interrogator is able to measure the strain or strain rate from this difference (Hartog, 2018).

The fact that DAS measures strain, or strain rate, and not particle velocity, particle acceleration or pressure like the more usual geophones, accelerometers and hydrophones, creates a doubt about the applicability of usual processing techniques and the results that can be obtained from this kind of data. For this reason some authors have proposed techniques to transform DAS data to geophone data. For example, Daley et al. (2016) probes the fibre response with a harmonic plane wave and arrives at a relationship between particle velocity v_z and strain rate $\dot{\epsilon}_{zz}$:

$$v_z = -c \int \dot{\epsilon}_{zz} dt, \tag{1}$$

where the z subindexes indicate the direction along the fibre and c is the apparent wave velocity along the fibre. Other transformation is Bóna et al. (2017), that proposes an equation for the DAS response, plugs a plane wave and solves the resulting expression in the wavenumber domain. Their transformation is a wavenumber domain filter:

$$\frac{-ik_z}{(1-e^{ik_zL})(1-e^{ik_zG})}, \tag{2}$$

where L is the laser pulse length, usually ignored, and G is the gauge length. As before, the subindex z indicates along the fibre.

The Containment and Monitoring Institute Field Research Station is research facility located in Alberta, Canada, where up to 400 tonnes of CO_2 are being injected annually into the ground for a 5 years period (Macquet et al., 2019). One of the technologies used to monitor this injection is DAS. There is a 5km loop of optical fibre permanently installed that runs inside a trench and two observation wells to record active and passive seismics (Lawton et al., 2017).

In this work we develop a least squares DAS to geophone transform based on DAS principles. First, we present the DAS basics. Then, we show how to create a linear system of equations between strain rate and vertical particle velocity from the basic theory. Following, we show how to propose a least squares inversion using the system of equations to obtain particle velocity from DAS measurements. Finally, we test this transformation with real data from CaMI-FRS, and compare some selected traces with the desired geophone data.

METHODS

DAS principles

The contents of this subsection are mainly based on Hartog (2018). A distributed acoustic sensing system is formed by the components shown in Figure 1. On the top of the figure, the laser generator sends laser pulses, in green, to the optical circulator that directs them to the sensing fibre. In the middle, two sections of the fibre, labelled A and B, that are separated by the distance L_G, also called gauge length, are probed by the laser pulse. The objective is to measure the axial strain between any pair of zones separated by a gauge length, like A and B. When the laser pulse arrives at section A, some of its energy is backscattered by the fibre inhomogeneities. This pulse is depicted in red. A brief moment later, the same happens at section B; this other backscattered pulse is shown in blue.

Both backscattered pulses are directed by the optical circulator towards the interferometer. The pulse from A arrives first and is optically duplicated with one copy taking the short path on the bottom and another taking the long path with a loop on top. The length of this loop is related to the gauge length L_G in the following way. When the pulse from section B is also duplicated, the copy that takes the short path through the interferometer aligns with the copy coming from section A that took the long path, as the bottom part of Figure 1 shows.

The result is that copies of both backscattered pulses from any sections A and B separated by a gauge length arrive at the same time at the end of the interferometer where their

interference pattern is generated. To be precise, what is detected is the interference pattern of the electrical fields of both pulses. Their mathematical expressions are:

$$E_A = E_{0A}\exp(i(\omega t + \Phi_A)) \quad (3)$$
$$E_B = E_{0B}\exp(i(\omega t + \Phi_B)), \quad (4)$$

where E_{0A} and E_{0B} are the field amplitudes, ω is the angular frequency, and Φ_A and Φ_B are the static phases. These phases are random due to the distribution of inhomogeneities at sections A and B, but also stable during the DAS operation. They are determined before the acquisition during the DAS calibration stage.

When a passing wavefield perturbs the fibre between A and B, the fibre contracts or dilates. The electrical field of the signal coming from section B is also perturbed in the following way:

$$E_{Bd} = E_{0B}\exp(i(\omega t + \Phi_{Bd})) \quad (5)$$
$$= E_{0B}\exp(i(\omega t + \Phi_B + \frac{4\pi n\xi\delta l}{\lambda})), \quad (6)$$

where the perturbed phase Φ_{Bd} is the summation of the static phase Φ_B and a term that contains the fibre refraction index n, a constant ξ that depends on the fibre properties, the pulse wavelength λ and the fibre change of length δl between zones A and B caused by the strain. The aim is to determine this δl from the interference pattern I_{AB}:

$$I_{AB} = (E_A + E_{Bd})(E_A + E_{Bd})^* \quad (7)$$
$$= E_{0A}^2 + E_{0B}^2 + 2E_{0A}E_{0B}\exp(i(\Phi_A - \Phi_B + \frac{4\pi n\xi\delta l}{\lambda})). \quad (8)$$

In this expression, the only unknown is δl that can be solved by the phase computation stage in Figure 1. Once δl is determined, it is divided by the gauge length to obtain the total tangent strain along this fibre portion and then assigned to the middle point s between A and B:

$$\epsilon_f(s) = \frac{\delta l}{L_G} \quad (9)$$

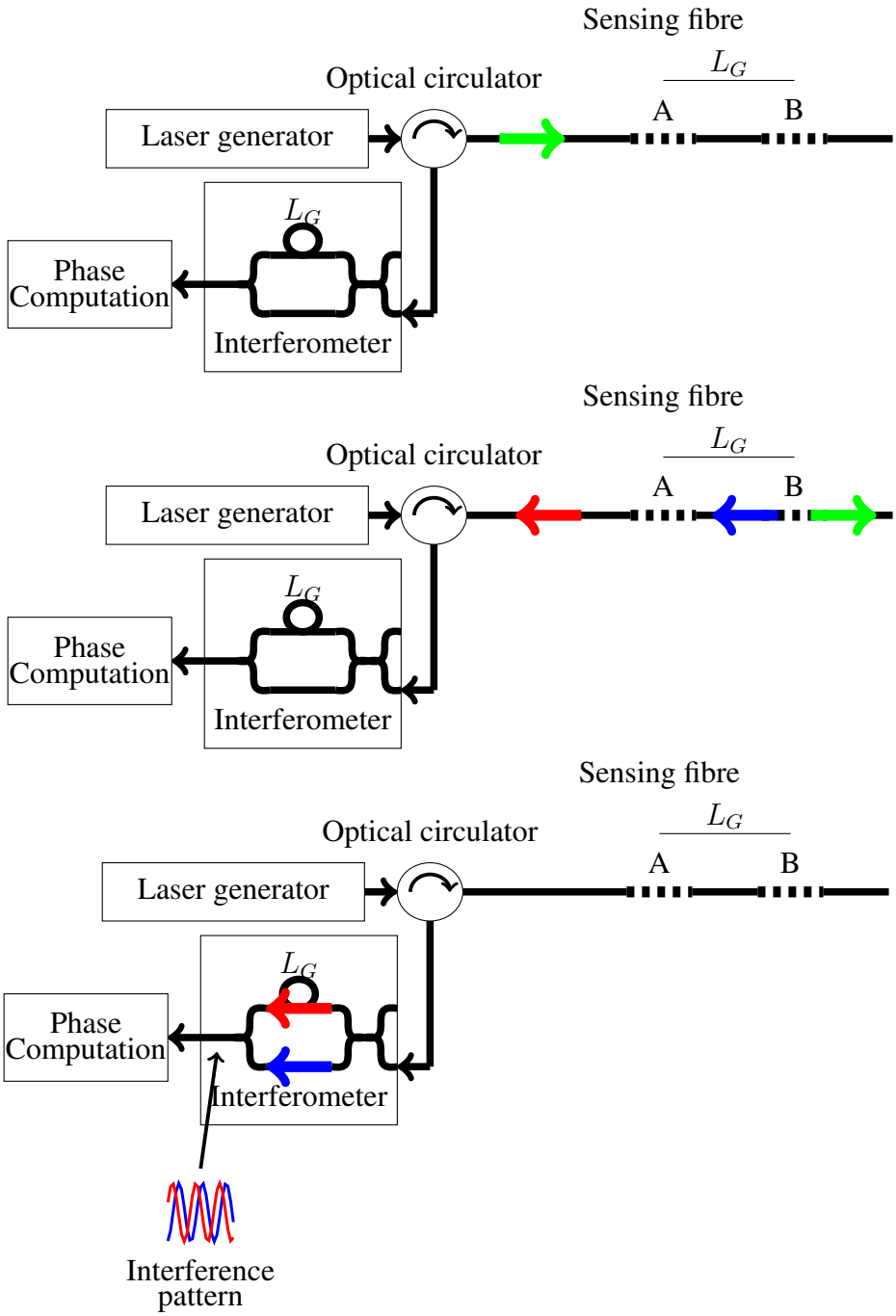

FIG. 1. Distributed acoustic sensing measuring principle. Their components are the laser generator that sends laser pulses to the sensing fibre through the optical circulator. The optical circulator also directs all backscattered pulses from the fibre to the interferometer. In addition, the interferometer output is connected to the phase computation stage. On the top, a laser pulse, in green, is sent to the fibre. In the middle, backscattered pulses, in red and blue, at two zones separated by a distance L_G return to the optical circulator. In the bottom, both backscattered pulses are aligned at the interferometer output where their interference pattern is generated. The objective is to use this interference pattern to calculate the axial strain between any pair of zones separated by a gauge length, like A and B.

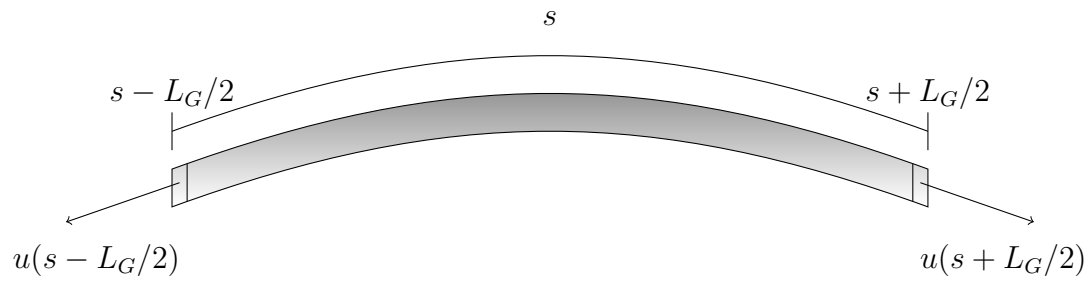

FIG. 2. Displacements along a portion of fibre of length L_G, the gauge length, centred around point s. The total dilation or contraction of this fibre portion detected by the interferometer is the difference between the displacements u along the fibre at both ends.

Particle velocity to strain rate linear system

Figure 2 shows a fibre section around point s of length G_L. The total change in length, δl of this section is related to the difference between the tangential displacements u at both ends of the section:

$$\delta l(s) = u(s + L_G/2) - u(s - L_G/2). \tag{10}$$

By replacing this in equation 9 we obtain an expression for the fibre strain in terms of displacement:

$$\epsilon_f(s) = \frac{1}{L_G}(u(s + L_G/2) - u(s - L_G/2)). \tag{11}$$

Furthermore, as many DAS systems measure strain rate instead of just strain, we can derive in time this last equation:

$$\dot{\epsilon}_f(s) = \frac{1}{L_G}(v(s + L_G/2) - v(s - L_G/2)), \tag{12}$$

where v is the tangential particle velocity. This tangential particle velocity can be obtained from the general three dimensional particle velocity $\vec{\boldsymbol{v}}$ vector by a projection along the fibre unit tangent vector $\vec{\boldsymbol{t}}$:

$$v(s) = \vec{\boldsymbol{t}}(s) \cdot \vec{\boldsymbol{v}}(s) \tag{13}$$

After replacing this last expression in equation 12 we obtain the general expression for strain rate in terms of particle velocity:

$$\dot{\epsilon}_f(s) = \frac{1}{L_G}(\vec{\boldsymbol{t}}(s + L_G/2) \cdot \vec{\boldsymbol{v}}(s + L_G/2) - \vec{\boldsymbol{t}}(s - L_G/2) \cdot \vec{\boldsymbol{v}}(s - L_G/2)) \tag{14}$$

We are interested primarily in DAS installed in vertical seismic profiles (VSP). In this survey configuration the fibre is installed vertically. This means that the only non zero component of the tangent vector $\vec{\boldsymbol{t}}$ is $t_z = 1$. Using this, the expression for strain rate in DAS VSP reduces to:

$$\dot{\epsilon}_f(s) = \frac{1}{L_G}(v_z(s + L_G/2) - v_z(s - L_G/2)), \tag{15}$$

where v_z is the vertical particle velocity. This expression is also used in Hall et al. (2020) to transform particle velocity to strain rate data.

The next step is to assemble a linear system of equations by considering every fibre portion of length L_G where DAS measured the strain rate. We suppose that DAS measured at points s_i, with $i = 1, \ldots, M$, along the fibre, for some integer M. We also assume that the distance between consecutive points s_i is Δs and that the gauge length $L_G = N\Delta s$ for some integer N. With this in mind, equation 15 is discretized in the following way:

$$\dot{\epsilon}_f(s_i) = \frac{1}{L_G}(v_z(s_{i+N/2}) - v_z(s_{i-N/2})). \tag{16}$$

Notice that additional points s_j with $j = 1 - N/2, \ldots, 0$ and s_k with $k = M + 1, \ldots, M + N/2$ are needed for this equation at the first and last points along the fibre. Finally, all discretized equations are assembled in a linear system:

$$\begin{bmatrix} \dot{\epsilon}_f(s_1) \\ \vdots \\ \dot{\epsilon}_f(s_i) \\ \vdots \\ \dot{\epsilon}_f(s_M) \end{bmatrix} = \frac{1}{L_G} \begin{bmatrix} -1 & 0 & \cdots & 0 & 1 & 0 & \cdots & 0 \\ 0 & -1 & 0 & \cdots & 0 & 1 & \cdots & 0 \\ \vdots & & & \ddots & & & & \vdots \\ 0 & \cdots & 0 & -1 & 0 & \cdots & 0 & 1 \end{bmatrix} \begin{bmatrix} v_z(s_{1-N/2}) \\ \vdots \\ v_z(s_i) \\ \vdots \\ v_z(s_{M+N/2}) \end{bmatrix} \tag{17}$$

Strain rate to particle velocity inversion

The linear system of equation 17 follows the common pattern where the measured data, strain rate, depends linearly of the model parameters, the vertical particle velocity. This system is usually written as:

$$\vec{\boldsymbol{d}} \;=\; G\vec{\boldsymbol{m}}, \tag{18}$$

where $\vec{\boldsymbol{d}}$ is the vector of strain rates, G is the matrix of equation 17 and $\vec{\boldsymbol{m}}$ are the vertical particle velocities. In order to regularize the solution of this system we expand it as:

$$\begin{bmatrix} G \\ \epsilon R \end{bmatrix} \vec{\boldsymbol{m}} \;=\; \begin{bmatrix} \vec{\boldsymbol{d}} \\ \vec{\mathbf{0}} \end{bmatrix}, \tag{19}$$

where operator R is the identity operator if we want to obtain the smallest model, or is the derivative operator if we want to obtain the flattest model (Aster et al., 2019), and ϵ is the regularization weight. We solve this system by using the conjugate gradient least squares method (Aster et al., 2019) with the Claerbout's conjugate gradient iteration step (Claerbout, 2008).

EXPERIMENTS

We tested the least squares DAS to geophone transform in DAS data from one of the CaMI-FRS observation wells. The top part of Figure 3 shows a DAS shot gather from one of the wells. The gauge length is 10m and the trace sampling is 0.25cm. The source was an Envirovibe located on the surface close to the wellhead with a linear sweep of 10 to 150Hz.

The middle and bottom parts of the Figure 3 show the two inversion results, the smallest and the flattest, product of the two different regularization operators in equation 19. Something to notice is the small horizontal shift to the right, for example at 0.1s and 250m, in the inverted shots due to the calculation of the strain rate at a point in terms of particle velocity at two other points half gauge length apart in both directions (equation 15). In this case, from the strain rate at any position during the first break, the inversion obtains two particle velocity values where one of them is in a fibre position where the fibre has not reacted yet to the wave first arrival.

The shape of the first arrival also changes in both inversions from a front lobed wavelet to a more zero phased one. Although less noticeable, the shape of the upgoing events also changes, for example just above 0.2s and 150m. However, downgoing events seem to be unchanged.

Figure 4 exhibits the corresponding vertical geophone data. In the observation well the geophones are installed from 191m to 306m depth every 5m. The top part of the figure is the original shot gather. The inverted gathers from Figure 3 do not look very similar to this gather. However, the bottom part shows a filtered version, with a 50 low cut, that is more similar to the inverted DAS gathers.

Figure 5 shows selected traces from the vertical geophone, DAS and inverted datasets. The geophone traces are at 191m depth. For registration purposes the DAS traces are at

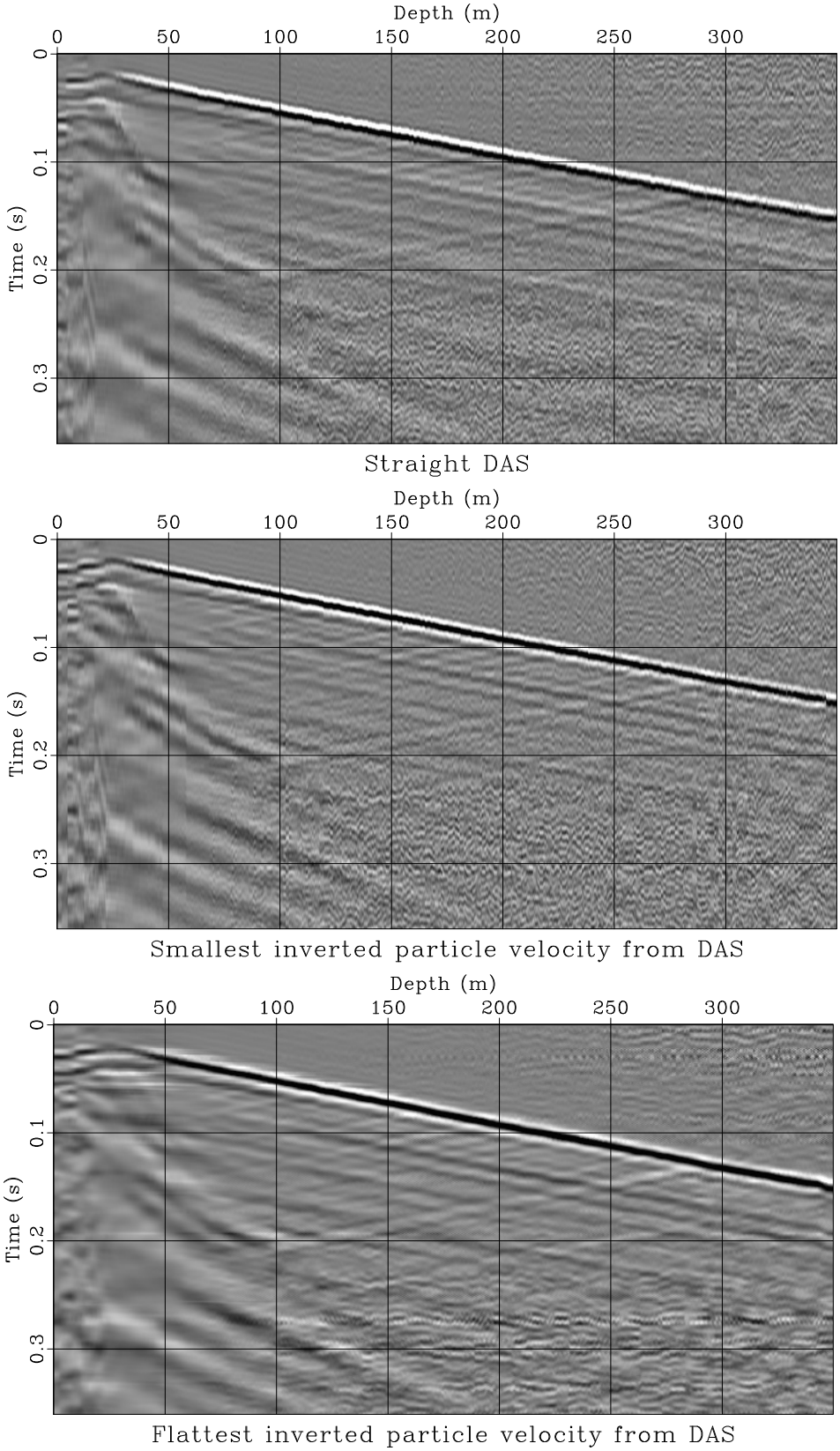

FIG. 3. The top part is a straight DAS vertical seismic profile shot gather from the Containment and Monitoring Institute Field Research Station (CaMI-FRS). The middle shows the vertical particle velocity inverted from the DAS data using the identity operator as regularization operator to obtain the smallest particle velocity model. The bottom part is the same inversion but using a derivative regularization operator to recover the flattest particle velocity model.

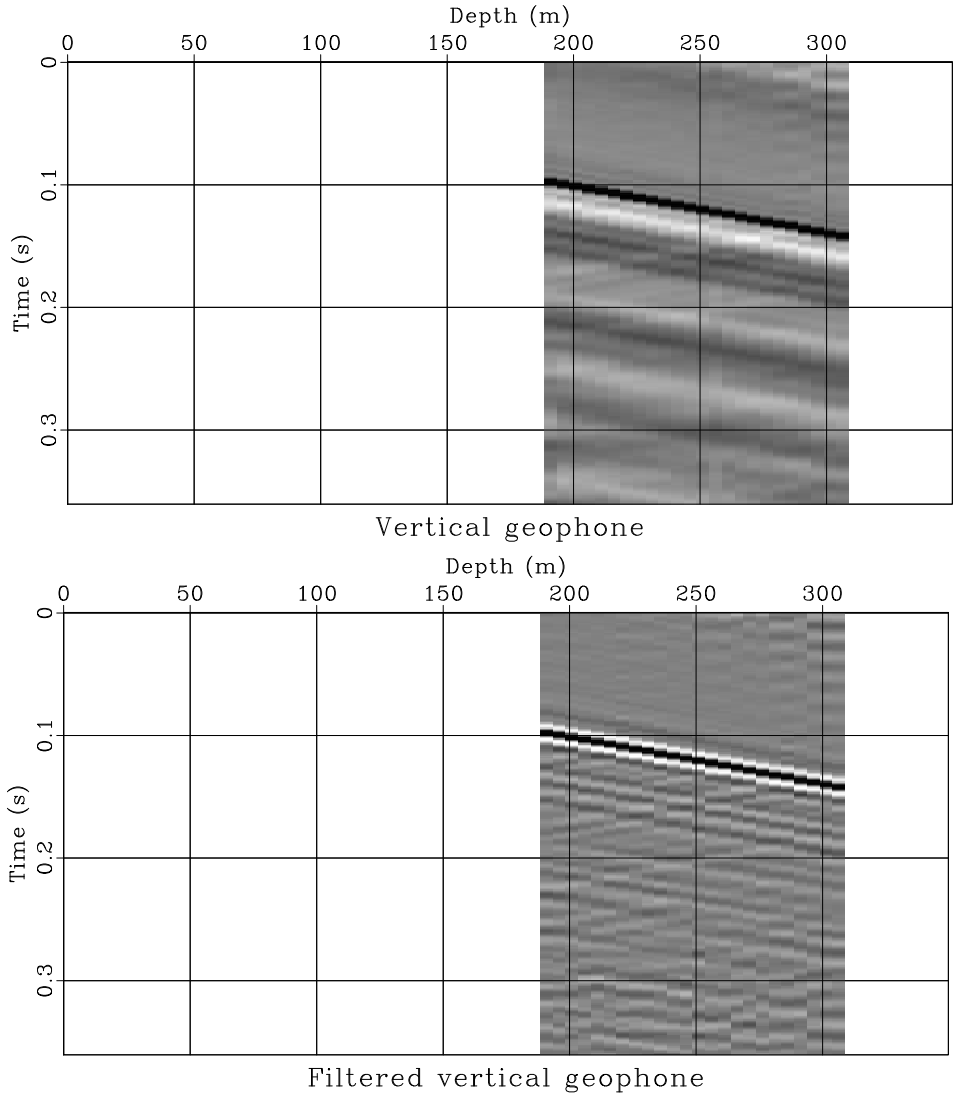

FIG. 4. Vertical geophone shot gather corresponding the the DAS shot gather of Figure 3. Geophones are installed in the observation well from 191m to 306m depth every 5m. The top part is the original data and the bottom is a 50Hz low cut filtered version.

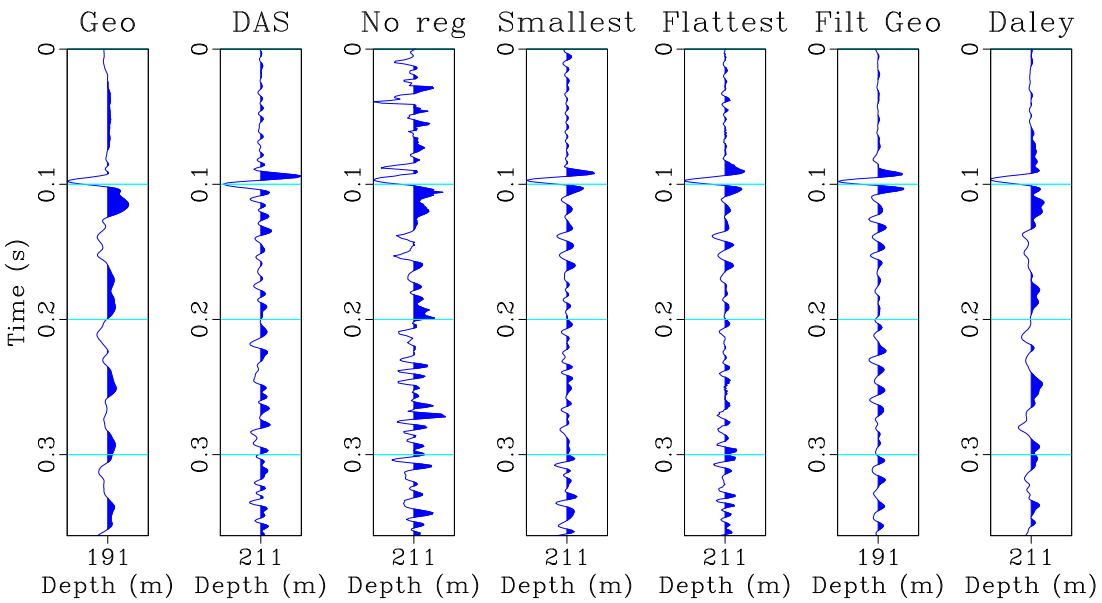

FIG. 5. Selected traces from the vertical geophone, DAS and inverted datasets. Geophone traces are at 191m depth in the well while DAS traces are at 211m along the fibre. From left to right, the first trace is the geophone response. The second is the DAS response. The third is the inverted geophone response from the DAS data without using regularization. The fourth solves for the smallest model while the five solves for the flattest one. The sixth trace is the high frequency part of the geophone response. The last one is the Daley transform of the DAS trace.

211m along the fibre. The first trace is the geophone trace while the second is the DAS one. Notice the difference in the first arrival character and the overall higher frequency content of the DAS trace.

The next group of traces are from the least squares inversion technique describe earlier. The third trace is the result with no regularization. The noise before the first break has been amplified, the first arrival looks similar to the geophone one and it seems like a noisy version of the geophone trace, at least before 0.2s. The fourth trace is the inversion result regularized to obtain the smallest model. It has less noise before the first break and a first arrival similar to the geophone one. However, the rest of the trace has little resemblance to the geophone trace. The fifth trace comes from the inversion regularized to obtain the flattest solution. It has similar characteristics to the smallest inverted model.

The sixth trace is a filtered version of the geophone trace. Specifically, the band below 50Hz is suppressed. This version of the geophone trace is more akin to the regularized inversion results in traces four and five. Finally, the last trace is the Daley transformation (equation 1) of the DAS trace. It looks highly similar to the original geophone trace.

DISCUSSION

The least squares DAS to geophone transformation presented is based in a linear operator that follows the description of the DAS inner workings that has been published (Hartog, 2018). However, there are many details that are proprietary and are not being included in the linear operator. For example, the patent Mahmoud et al. (European patent

EP2435796B1, May. 2010) uses visibility factors to calculate a better acoustic perturbation. DAS aspects no modelled can be difficult to invert.

The inversion results of Figure 3 are more similar to the high frequency version of the corresponding geophone data in Figure 4. This can also be seen in the individual traces in Figure 5. One explanation is that there is a low frequency aspect missing in the linear operator that prevents us for invert that part of the trace.

In addition, the part of the inverted DAS traces that resembles more the filtered geophone trace is the early times. Later times look different. It is reported that DAS data has less signal to noise ratio than geophone data (Gordon, 2019). The early part of the trace is usually less affected by the noise and provides a better dataset to invert.

The Daley transform Daley et al. (2016) produced a better result that the least squares method. Again, this can be the result of a missing part in the modelling operator. However, the original version of the geophone shot gather in Figure 4 has low frequency components that mask most of the upgoing events that are more evident in the filtered version in the same figure.

The trace inverted without regularization in Figure 5 shows that regularization is important in this inversion. We used two very common regularization operators, but there are others that could be more appropriate.

The least squares inversion shifted the traces to the right as explained in Figure 3 due to the gauge length in the modelling operator. This shift to the right makes the events in the corridor stack deeper. It has been reported that the corridor stack of this DAS dataset locates the events at a more shallow depth that the geophone corridor stack (Gordon, 2019).

CONCLUSIONS

The least squares DAS to geophone transformation is based on a linear modelling operator that includes most of the DAS aspects. However, it is possible that some part is not modelled.

The least squares DAS to geophone transformation was able to invert the early times and the high frequency part of the geophone trace. In this aspect is of less quality than the Daley transformation.

The regularization is fundamental in the least squares transformation. Without it the noise before first arrivals was amplified.

ACKNOWLEDGEMENTS

We thank the sponsors of CREWES and the CaMI.FRS JIP subscribers for continued support. This work was funded by CREWES industrial sponsors and CaMI.FRS JIP subscribers, NSERC (Natural Science and Engineering Research Council of Canada) through

the grants CRDPJ 461179-13 and CRDPJ 543578-19. Partial funding also came from the Canada First Research Excellence Fund. The data were acquired at the Containment and Monitoring Institute Field Research Station in Newell County AB, which is part of Carbon Management Canada.

REFERENCES

Aster, R., Borchers, B., and Thurber, C., 2019, Parameter Estimation and Inverse Problems (Third Edition): Elsevier, third edition edn.
URL http://www.sciencedirect.com/science/article/pii/B9780128046517000055

Bóna, A., Dean, T., Correa, J., Pevzner, R., Tertyshnikov, K., and Zaanen, L., 2017, Amplitude and phase response of DAS receivers, *in* 79th EAGE Conference and Exhibition 2017, http://earthdoc.eage.org/publication/publicationdetails/?publication=88917.

Claerbout, J. F., 2008, Image estimation by example:
URL http://sepwww.stanford.edu/sep/prof/gee8.08.pdf

Daley, T., Miller, D., Dodds, K., Cook, P., and Freifeld, B., 2016, Field testing of modular borehole monitoring with simultaneous distributed acoustic sensing and geophone vertical seismic profiles at Citronelle, Alabama: Geophysical Prospecting, **64**, No. 5, 1318–1334, https://onlinelibrary.wiley.com/doi/pdf/10.1111/1365-2478.12324.

Daley, T. M., Freifeld, B. M., Ajo-Franklin, J., Dou, S., Pevzner, R., Shulakova, V., Kashikar, S., Miller, D. E., Goetz, J., Henninges, J., and Lueth, S., 2013, Field testing of fiber-optic distributed acoustic sensing (DAS) for subsurface seismic monitoring: The Leading Edge, **32**, No. 6, 699–706, https://doi.org/10.1190/tle32060699.1.

Gordon, A. J., 2019, Processing of DAS and geophone VSP data from the CaMI Field Research Station: M.Sc. thesis, University of Calgary, https://prism.ucalgary.ca/handle/1880/110175?

Hall, K. W., Innanen, K. A., and Lawton, D. C., 2020, Comparison of multi-component seismic data to fibre-optic (DAS) data, 525–529, https://library.seg.org/doi/pdf/10.1190/segam2020-3427754.1.
URL https://library.seg.org/doi/abs/10.1190/segam2020-3427754.1

Hartog, A. H., 2018, An introduction to distributed optical fibre sensors: CRC Press.

Lawton, D., Bertram, M., Saeedfar, A., Macquet, M., Hall, K., Bertram, K., Innanen, K., and Isaac, H., 2017, DAS and seismic installations at the CaMI Field Research Station, Newell County, Alberta, Tech. rep., CREWES, https://www.crewes.org/ForOurSponsors/ResearchReports/2017/CRR201751.pdf.

Macquet, M., Lawton, D. C., Saeedfar, A., and Osadetz, K. G., 2019, A feasibility study for detection thresholds of CO2 at shallow depths at the CaMI Field Research Station, Newell County, Alberta, Canada: Petroleum Geoscience, **25**, No. 4, 509–518, https://pg.lyellcollection.org/content/25/4/509.full.pdf.

Mahmoud, F., Richard, P. T., and Sergey, S., European patent EP2435796B1, May. 2010, Optical sensor and method of use.